J. Fluid Mech. (2000), *vol.* 402, *pp.* 195–210. Printed in the United Kingdom

© 2000 Cambridge University Press

A simple hydrodynamic model for transition boiling

By SANG W. JOO[1]† STEPHEN H. DAVIS[1] AND S. GEORGE BANKOFF[2]

[1]Department of Engineering Sciences and Applied Mathematics, Northwestern University, Evanston, IL 60208, USA

[2]Department of Chemical Engineering, Northwestern University, Evanston, IL 60208, USA

(Received 26 March 1999 and in revised form 30 July 1999)

A vertical column of an inviscid fluid, heated uniformly from below through a horizontal rigid bottom, is studied, with focus on the dynamics of the vapour/liquid interface near the three-phase (contact) line. The interfacial motion is induced by the competing effects of liquid feeding from above and evaporative mass loss through the interface. A linearized solution is obtained that describes the location of the contact line. The solution is used to study the transition processes to and from film boiling, where part of the liquid, lying on top of a vapour layer, can spontaneously be drawn downward and touch the heated bottom. Recession or advancement of the contact line then determines whether the film boiling is sustained or broken. It is seen that the correct contact-line dynamics cannot be predicted solely from a global mass balance in the liquid column.

1. Introduction

When a pool of liquid is heated from below beyond a critical temperature, a complex sequence of boiling phenomena occur as the superheat is increased. The states are usually classified as natural convection, nucleate boiling, transition boiling, and film boiling, in the order they appear as the heating intensity is increased, and have been studied intensively, as reviewed by Rohsenow (1971), by Dhir (1998), and in a monograph by Carey (1992) among many others. We shall not repeat the discussions of these immense areas, but rather provide here a focused view that prompted the present study.

In nucleate boiling vapour bubbles are created at the heated bottom, which grow, merge, and launch as the process develops. Due to the works by Snyder & Edwards (1956), Moore & Mesler (1961), and Cooper & Lloyd (1969), it is believed that a microlayer exists between the bubble surface (vapour/liquid interface) and the heated bottom. The heated bottom thus is mostly in direct contact with liquid. The contribution of this microlayer to evaporation and, in turn, to the heat-transfer characteristics is a subject of many recent investigations, including that by Wilson, Davis & Bankoff (1999).

When the superheat is sufficiently large, the film-boiling state is reached, where the liquid is no longer in contact with the heated bottom, but is separated by a

† Permanent address: School of Mechanical Engineering, Yeungnam University, Gyongsan 712-749 Korea.

https://doi.org/10.1017/S0022112099006758 Published online by Cambridge University Press

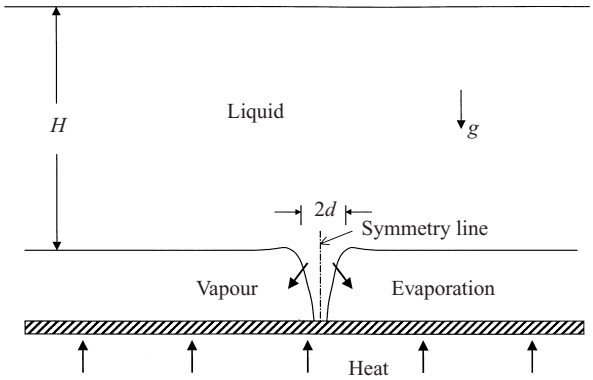


FIGURE 1. A schematic configuration for boiling near the lower critical heat flux. (Vertical scale of the vapour phase highly exaggerated.)

continuous film of the vapour. Film boiling has been relatively amenable to more straightforward studies, as discussed in the aforementioned reviews.

Between the 'fully developed' nucleate boiling and the onset of the film boiling there is a transition state, where the swapping of the phases in contact with the heated bottom should occur. The liquid phase (the microlayer and the bulk) recedes and is gradually displaced by the vapour phase at the heated bottom. If the superheat is decreased from the film-boiling state, the reverse will occur. In this regime, the heat flux decreases with the increase of the bottom temperature, so that there is a minimum heat flux near the onset of the film boiling, usually called the lower critical heat flux. One of the more important recent needs in the study of transition boiling (also called partial film boiling) is an accurate assessment of this lower critical heat flux, which requires more rigorous analyses and careful observations on the wetting/dewetting process, or the evolution of the vapour/liquid interface near the heated bottom.

The experimental data of Witte & Lienhard (1982) on film boiling show that the liquid/solid-surface wetting characteristics alter the lower critical heat flux and thus the critical superheat for a sustained film boiling. They indicate that at least near the lower temperature end of the film boiling intermittent contact between the liquid and the heated bottom occurs. Stability analysis (Panzarella 1998, for example) of the vapour liquid interface in film boiling also shows a spontaneous incipient rupture process of the vapour film. The liquid, upon touching the bottom (vapour-film rupture), may either spread (toward transition boiling) or vaporize (toward film boiling), depending upon the competitive effects of evaporation and feeding from the liquid bulk above. The dynamics of the wetting/dewetting process, or the liquid/solid contact, near the onset of film boiling again is a critical subject for investigation.

As a generic case for the aforementioned transition processes, we picture a film-boiling (or transition) state with a liquid 'finger' making a contact with a heated bottom, as shown in figure 1. The width of the finger and the depth of liquid bulk are 'roughly' $2d$ and H, respectively. If a film-boiling state were to be recovered, the tip of the liquid finger in contact with the bottom would narrow via evaporation sufficient to overcome the liquid flux downward from the bulk. The two contact lines would recede until they merge with each other, after which the finger tip would detach from the bottom, making the vapour film continuous. The opposite would be true for an evolution toward transition boiling. The contact lines would advance, resulting in the wetting of the heated bottom. The liquid flux from the bulk would dominate

https://doi.org/10.1017/S0022112099006758 Published online by Cambridge University Press

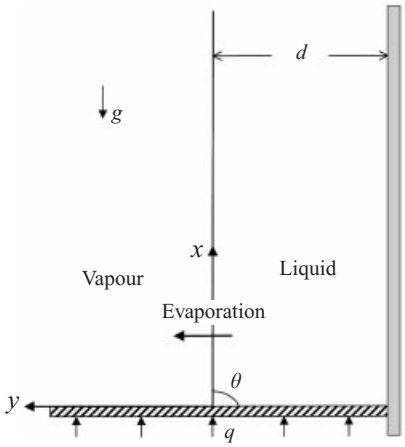


FIGURE 2. Flow configuration.

the evaporation mass flux across the vapour/liquid interface. In order to understand better the fundamental nature of these evolutions, we study here a model problem that captures the effects of evaporation mass flux and downward liquid flow due to gravity. We focus on the local behaviour of the finger near the heated bottom, and model it as a vertical inviscid liquid column extended infinitely upward from the bottom. The finger will be assumed to stay symmetric, so that no-flux conditions can be imposed along the symmetry line, which will be replaced by an insulating rigid wall. The pressure in the vapour phase will be considered uniform, and its dynamics decoupled from that of the liquid. In the following sections, we formulate this model problem (§ 2), obtain a uniformly valid analytical solution that describes the evolution of the vapour/liquid interface (§ 3), evaluate the solution to show boiling transitions (§ 4), and conclude in § 5.

2. Formulation

In transition and film boiling the characteristic Reynolds number is usually large. We thus consider an inviscid liquid, with constant density ρ, thermal conductivity k, and heat capacity c_p, bounded below by a rigid bottom and unbounded vertically upward. Laterally, it is bounded by an insulating rigid wall to the right and by the interface with its vapour phase to the left. The bottom plate is heated, and supplies a constant heat flux to the liquid. The heat is transferred away from the bottom, and is also lost across the vapour/liquid interface due to evaporation. Figure 2 shows the flow configuration, where the liquid (and so the interface) is as yet undisturbed from its initially uniform width d.

The flow in the liquid phase is described by the Laplace equation

$$\phi_{xx} + \phi_{yy} = 0 \quad \text{for} \quad x \geqslant 0, \quad -1 \leqslant y \leqslant h, \tag{2.1}$$

where the velocity potential $\phi(x, y, t)$ is measured in units of the thermal diffusivity κ of the liquid and the subscripts denote partial differentiation. Here x and y, in units of d, are directed vertically upward along the initial undisturbed vapour/liquid interface and toward the vapour phase along the heated bottom, respectively. The dimensionless time t is in units of d^2/κ. The location of the vapour/liquid interface $y = h(x, t)$ varies with time and space. The energy equation for the liquid phase is

https://doi.org/10.1017/S0022112099006758 Published online by Cambridge University Press

stated as

$$\frac{\mathrm{d}T}{\mathrm{d}t} = T_{xx} + T_{yy} \quad \text{for} \quad x \geqslant 0, \quad -1 \leqslant y \leqslant h, \tag{2.2}$$

where $\mathrm{d}/\mathrm{d}t = \partial_t + \phi_x\partial_x + \phi_y\partial_y$. The dimensionless temperature T measures the superheat relative to the latent heat L:

$$T \equiv \rho c_p \left(\check{T} - T_s\right)/L, \tag{2.3}$$

where $\check{T}$ and T_s are, respectively, dimensional and saturation temperatures.

On the bottom ($x = 0$) there is no penetration of the liquid

$$\phi_x = 0 \quad \text{on} \quad x = 0, \quad -1 \leqslant y \leqslant h, \tag{2.4}$$

and constant heat flux

$$-T_x = \epsilon \quad \text{on} \quad x = 0, \quad -1 \leqslant y \leqslant h, \tag{2.5}$$

where

$$\epsilon = \frac{\rho c_p dq}{kL} \tag{2.6}$$

measures the magnitude of the imposed heat flux q. On the insulated side ($y = -1$) there is zero flux of mass and heat,

$$\phi_y = T_y = 0 \quad \text{on} \quad y = -1. \tag{2.7}$$

On the vapour/liquid interface $y = h(x,t)$, the jump in normal traction is balanced by the capillary force and the vapour thrust, which can be expressed through the Bernoulli equation,

$$\phi_t + \tfrac{1}{2}(\phi_x^2 + \phi_y^2) + \overline{G}h - S\frac{h_{xx}}{N^3} + DJ^2 = 0 \quad \text{on} \quad y = h, \tag{2.8}$$

where

$$\overline{G} = \frac{gd^3}{\kappa^2} \tag{2.9}$$

measures the initial width of the liquid, $J(x,t)$ is the non-dimensional evaporation mass flux, and $N = \sqrt{1 + h_x^2}$. The parameters,

$$S = \frac{\gamma d}{\rho\kappa^2}, \tag{2.10}$$

and

$$D = \frac{\rho}{\rho_V}, \tag{2.11}$$

measure the interfacial tension γ and the ratio of liquid to vapour (ρ_V) densities. The vapour thrust DJ^2 describes the extra stress exerted on the interface due to the evaporation; vapour particles, launching at substantially increased velocities upon phase change (due to the conservation of mass flux across the interface), apply normal stress on the interface. In (2.8) other dynamics of the vapour are ignored for $D \gg 1$. A detailed derivation for a viscous equivalent of this one-sided model is given by Burelbach, Bankoff & Davis (1988). The interface is not a material surface in the presence of the evaporation, and its mass balance is defined by

$$\phi_y - NJ = h_t + \phi_x h_x \quad \text{on} \quad y = h, \tag{2.12}$$

https://doi.org/10.1017/S0022112099006758 Published online by Cambridge University Press

where the mass flux J is directed into the vapour, positive (negative) for evaporation (condensation). The energy balance across the interface

$$NJ + T_y - T_x h_x = 0 \quad \text{on} \quad y = h \tag{2.13}$$

states that the heat conducted through the interface is used to vaporize the liquid particles. Here no heat conduction in the vapour phase is taken into account. A linear constitutive model

$$KJ = T \quad \text{on} \quad y = h \tag{2.14}$$

is adopted to relate the evaporation mass flux to local interface temperature. Here K measures the degree of non-equilibrium at the evaporating interface, and can be related to the kinetics of the vapour particles. A rigorous discussion of this constitutive model, including its limitations, is reported by, among others, Panzarella (1998), who also presents a more general constitutive equation. Another noteworthy discussion that can lead to the above interfacial conditions is given by Prosperetti & Plesset (1984).

Unless the capillary term in (2.8) is ignored, additional conditions must be specified at the contact line that relate the contact angle θ to other flow variables. For a non-material interface, the contact line can advance or recede solely due to mass flux across the interface. When the contact line is in motion, the dynamic contact angle can be substantially influenced by mass loss (Anderson & Davis 1995). For the present analysis we set

$$h_x = 0 \quad \text{at} \quad x = 0; \tag{2.15}$$

the contact angle θ is maintained at $\pi/2$. In the presence of the evaporation, this condition is not to be confused with the fixed-contact-angle condition for a material surface.

Initially the liquid is at rest, at uniform saturation temperature, and has a flat undisturbed vertical interface:

$$\phi = T = h = 0 \quad \text{for} \quad t < 0. \tag{2.16}$$

3. A uniformly valid solution

Noting that the superheat parameter ϵ is much smaller than unity, we expand the dependent variables in terms of ϵ:

$$\boldsymbol{W} = \epsilon \boldsymbol{W}_1 + \epsilon^2 \boldsymbol{W}_2 + \ldots, \tag{3.1}$$

where $\boldsymbol{W} = (\phi, T, h, J)$. While the other parameters are set to be of order unity, $\overline{G} = O(\epsilon)$, limiting the analysis valid for small enough liquid widths, and $D = o(\epsilon^{-1})$, eliminating the effect of vapour thrust from the leading-order behaviour.

At the leading order in ϵ, one obtains a linear system:

$$\varphi_{xx} + \varphi_{yy} = 0 \quad \text{for} \quad x \geqslant 0, \quad -1 \leqslant y \leqslant 0, \tag{3.2}$$

$$T_t = T_{xx} + T_{yy} \quad \text{for} \quad x \geqslant 0, \quad -1 \leqslant y \leqslant 0, \tag{3.3}$$

$$\varphi_x = Gt \quad \text{on} \quad x = 0, \quad -1 \leqslant y \leqslant 0, \tag{3.4}$$

$$T_{1x} = -1 \quad \text{on} \quad x = 0, \quad -1 \leqslant y \leqslant 0, \tag{3.5}$$

$$\varphi_y = T_{1y} = 0 \quad \text{on} \quad y = -1, \tag{3.6}$$

$$\varphi_t - S h_{1xx} = 0 \quad \text{on} \quad y = 0; \quad h_{1x} = 0 \quad \text{at} \quad x = 0, \tag{3.7}$$

https://doi.org/10.1017/S0022112099006758 Published online by Cambridge University Press

$$\varphi_y - J_1 = h_{1t} \quad \text{on} \quad y = 0, \tag{3.8}$$

$$T_1 + K T_{1y} = 0; \quad K J_1 = T_1 \quad \text{on} \quad y = 0, \tag{3.9}$$

$$\varphi_x \to 0, \quad h_1 \to 0, \quad T_1 \to 0 \quad \text{as} \quad x \to \infty, \tag{3.10}$$

$$\varphi = T_1 = h_1 = 0 \quad \text{for} \quad t < 0. \tag{3.11}$$

Here a new velocity potential $\varphi \equiv \phi_1 + Gxt$ has been introduced, which in effect translates the vertical downward flow from infinity into an equivalent upward bottom motion with no flow at infinity ($\varphi_x \to 0$ as $x \to \infty$ as above). A rescaled parameter G of order unity is used in place of $\overline{G}$ by taking $\overline{G} = \epsilon G$.

The bottom-boundary condition (3.4) describes the falling of the liquid column with a constant acceleration (free fall), since the fluid is inviscid. The mass flux of the liquid from infinity increases indefinitely in time, and will eventually dominate any evaporative mass flux into the vapour; the contact line will always advance after a sufficient amount of time, and the liquid will completely wet the heated bottom. In order to model situations in which the external flow and evaporation compete one must modify equation (3.4). For example

$$\varphi_x = Q\left(1 - \mathrm{e}^{-(G/Q)t}\right) \quad \text{on} \quad x = 0. \tag{3.12}$$

For small time, the speed increases with constant acceleration G as in (3.4), but instead of growing linearly forever, it asymptotes to a finite terminal value Q, which can be considered as an external parameter that determines the liquid feeding rate from infinity. If one wishes, one can relate this to the hydrostatic head that forces the liquid down through the base of the finger (of depth H) in figure 1,

$$Q = \frac{d}{\kappa}\sqrt{2gH}. \tag{3.13}$$

The parameter Q will be defined more accurately when this study is generalized to include the dynamics of the vapour phase.

It is to be noted that the above linear system resembles that for the linear inviscid wavemaker problem, where a rigid wall (the bottom in figure 2) translates parallel to the undisturbed free surface with a prescribed velocity. In the absence of evaporation ($J = 0$), the temperature field is decoupled, and the above is exactly the wavemaker problem in the absence of gravity. The wavemaker problem has been studied intensively as an important model problem for a contact-line singularity on a surface-piercing body in translation in the inviscid theory. Peregrine (1972) finds a logarithmic singularity (infinite displacement) at the contact line. Roberts (1987) obtained a non-singular local similarity solution near the contact line. It was later realized by Joo, Messiter & Schultz (1990) that a straightforward solution in a Fourier integral serves as a uniformly valid solution that recovers the local similarity solution near the contact line and the outer (Peregrine's) solution away from it. In the present study the solutions will be obtained for the above system in terms of Fourier integrals.

The temperature field at this leading order is purely diffusive, and is decoupled from the flow field. The solution for (3.3) with the boundary conditions (3.5), (3.6), and (3.9) that satisfies (3.10) and (3.11) is expressed as

$$T_1 = \frac{2}{\pi}\sum_{n=1}^{\infty} \cos\lambda_n(y+1) \int_0^{\infty} F_{1n}(k,t)\cos kx \,\mathrm{d}k, \tag{3.14}$$

https://doi.org/10.1017/S0022112099006758 Published online by Cambridge University Press

where the eigenvalues λ_n are obtained from

$$\cos\lambda - K\lambda_n \tan\lambda_n = 0 \tag{3.15}$$

and

$$F_{1n} = \frac{4\sin\lambda_n}{(\lambda_n^2 + k^2)(2\lambda_n + \sin 2\lambda_n)}\left[1 - \mathrm{e}^{-(\lambda_n^2+k^2)t}\right]. \tag{3.16}$$

The evaporative mass flux then is obtained from (3.9) as

$$J_1 = \frac{2}{\pi}\int_0^\infty \sum_{n=1}^\infty F_{2n}\cos kx\,\mathrm{d}k, \tag{3.17}$$

where

$$F_{2n} = \frac{2\sin^2\lambda_n}{(\lambda_n^2 + k^2)(1 + K\sin^2\lambda_n)}\left[1 - \mathrm{e}^{-(\lambda_n^2+k^2)t}\right]. \tag{3.18}$$

Through the linearization of (3.9) the dependence of the temperature field on the interface configuration is eliminated, so that the evaporative mass flux is independent of h_1.

In solving (3.2) with the remaining conditions, we write

$$\varphi = \frac{2}{\pi}\int_0^\infty \breve{\varphi}\cos kx\,\mathrm{d}k, \tag{3.19}$$

and

$$h_1 = \frac{2}{\pi}\int_0^\infty B(k,t)\cos kx\,\mathrm{d}k. \tag{3.20}$$

The Fourier cosine transformation $\breve{\varphi}$, compatible with (3.6) and (3.12), must be written as

$$\breve{\varphi} = A(k,t)\cosh k(y+1) - \frac{Q}{k^2}\left(1 - \mathrm{e}^{-(G/Q)t}\right). \tag{3.21}$$

The interfacial boundary conditions (3.7) and (3.8) then yield a coupled system of equations for A and B:

$$A_t\cosh k + Sk^2 B = \frac{G}{k^2}\mathrm{e}^{-(G/Q)t}, \tag{3.22}$$

$$Ak\sinh k - \sum_{n=1}^\infty F_{2n} = B_t. \tag{3.23}$$

A can be eliminated between these, giving rise to a single ordinary differential equation for the Fourier cosine transform $B(k,t)$ of the interface configuration:

$$B_{tt} + \beta^2 B = G\mathrm{e}^{-(G/Q)t}\frac{\tanh k}{k} - \sum_{n=0}^\infty \frac{2\sin^2\lambda_n}{1 + K\sin^2\lambda_n}\mathrm{e}^{-(\lambda_n^2+k^2)t}, \tag{3.24}$$

where

$$\beta = k\sqrt{Sk\tanh k}. \tag{3.25}$$

The initial conditions (3.11) for φ and h_1 provide those for B:

$$B(k,0) = B_t(k,0) = 0. \tag{3.26}$$

The solution to the linear equation (3.24) can finally be obtained as

$$B = B_1 + B_2, \tag{3.27}$$

https://doi.org/10.1017/S0022112099006758 Published online by Cambridge University Press

where the isothermal contribution

$$B_1 = \frac{G}{(G/Q)^2+\beta^2}\frac{\tanh k}{k}\left(\mathrm{e}^{-(G/Q)t} - \cos\beta t + \frac{G}{Q}\frac{\sin\beta t}{\beta}\right) \tag{3.28}$$

is due to the bottom translation (or the liquid flux from infinity) and

$$B_2 = \sum_{n=1}^{\infty}\left[\cos\beta t - (\lambda^2+k^2)\frac{\sin\beta t}{\beta} - \mathrm{e}^{-(\lambda_n^2+k^2)t}\right]\frac{1}{(\lambda_n^2+k^2)^2+\beta^2}\frac{2\sin^2\lambda_n}{1+K\sin^2\lambda_n} \tag{3.29}$$

governs the effect of evaporation mass flux on the interface configuration.

Using B and consequently A, the interface configuration h and other flow variables can be completely described in terms of Fourier integrals. In the following section, the integral for h is evaluated numerically in order to examine the interface evolution near the heated base.

4. Evaluation of the interface configuration

The Fourier cosine integral (3.20) is evaluated by an adaptive method that uses 10-point Gauss–Legendre and 21-point Kronrod formulae with automatic subinterval adjustment with maximum absolute error of 10^{-9} for small to moderate k and Filon's method for sufficiently large k to capture rapid oscillations of the integrand accurately.

The parameters to consider are K, Q, G, S, which are related to reciprocal evaporation intensity, liquid feeding from infinity, width of the liquid column (or 'finger'), and interface tension, respectively. It can be easily seen from (3.9) that $K = \infty$ ($K = 0$) corresponds to zero (maximum) evaporation. When $K = \infty$ the interface behaves as an insulating surface, and heat from the bottom is transferred vertically upward. No evaporation would occur. On the other hand, when $K = 0$, heat transferred to the interface is instantly used for vaporization. The interfacial temperature remains at the saturation value, and the evaporation mass flux is maximized. The values $K = 0, 1, 100$ will be used below for strong, moderate, and weak evaporation, respectively, for illustrative purposes. The parameter Q is also varied from zero (no feeding from infinity, or pure evaporation) to 10 (high feeding rate). The parameter G only affects the transient flow, and thus is set to unity for convenience. The linear system listed in the previous section can easily be rescaled to eliminate the parameter S, and so one can set $S = 1$.†

Figure 3 shows instantaneous interface configurations of a liquid column for different times when there is no liquid feeding from infinity ($Q = 0$). The interfacial deformation is purely due to evaporation. The evaporative mass loss is strongest at the contact line, and since no liquid is supplied from above, there is monotonic mass loss. The contact line thus would recede with time indefinitely. The recession of the interface near the contact line generates capillary waves that travel away from the base. As the depletion near the contact line increases with time, this wave grows in time. The amplitudes of the humps appear most pronounced near the bottom, and decay monotonically away from it. Interfacial configurations for smaller times are shown in a magnified view in (*b*). The evolving configurations of the interface shown suggest the possibility of a local similarity solution.

† In the linear system (3.2)–(3.12) the interfacial-tension parameter S can be eliminated by setting $x = S\xi, \quad y = S\eta, \quad t = S^2\tau$ and rewriting the system in terms of the new independent variables (ξ, η, τ). It is seen then that h_1 and J_1 are replaced with h_1/S and J_1/S, respectively, and the parameters (K, Q) with (SK, Q/S).

https://doi.org/10.1017/S0022112099006758 Published online by Cambridge University Press

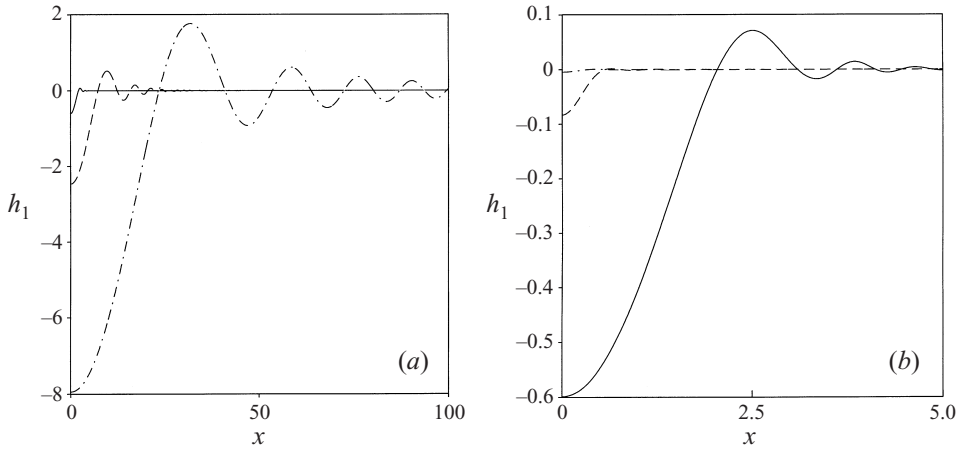


FIGURE 3. Interface configurations for pure evaporation: $Q = 0$, $S = K = 1$. (*a*) Three different times, $t = 1$ (——), $t = 10$ (- - - -) and $t = 100$ (– · –); (*b*) magnified view for $t = 0.1$ (- - - -) and $t = 1$ (——).

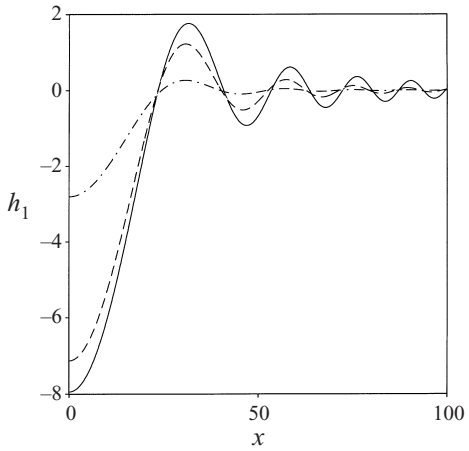


FIGURE 4. Interfacial configurations at a large time for pure evaporation: $Q = 0$. $S = 1$, $t = 100$, and $K = 0$ (——), $K = 1$ (- - - -) and $K = 100$ (– · –).

In figure 4 interface configurations for pure evaporation ($Q = 0$) are shown again for three different values for K at a sufficiently large time. As mentioned above, $K = 0$ shows the highest rate of evaporation, and thus the most pronounced contact-line recession. With weak evaporation, there is apparently no deflection of the interface. A more detailed figure (not shown here) clearly shows the capillary wave, albeit with small amplitude. The phase speed of the wave seems to decrease only slightly with K.

The location of the contact line for pure evaporation is plotted against time in figure 5 for three different values for K. In all cases shown, the contact-line height decreases monotonically and seems to equilibrate to a constant rate (speed) for sufficiently large time. It is expected that the contact line eventually will reach the right-hand boundary $y = -1$ (merging of the contact lines receding from the two sides of the symmetry line), which, however, cannot be predicted accurately by a linear theory.

https://doi.org/10.1017/S0022112099006758 Published online by Cambridge University Press

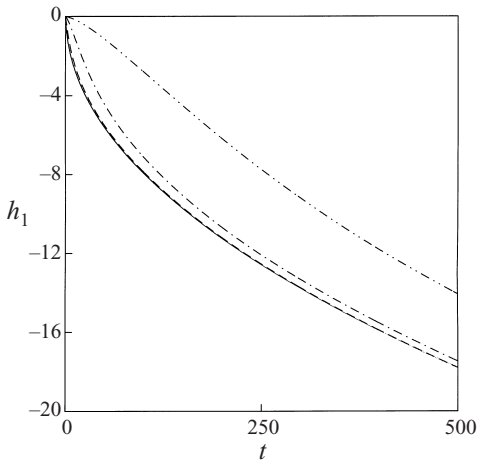


FIGURE 5. Contact-line motion for pure evaporation: $Q = 0$. $S = 1$, and $K = 0$ (——), $K = 0.1$ (- - - -), $K = 10$ (– · –) and $K = 100$ (— ··—).

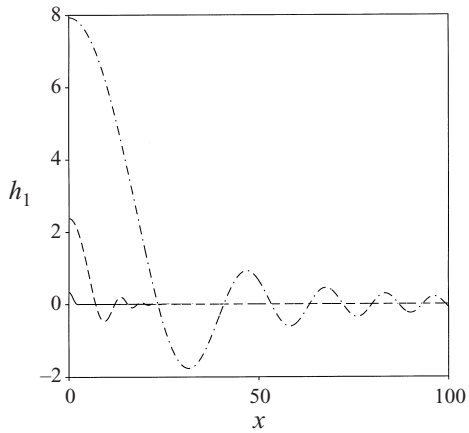


FIGURE 6. Interface configurations for an isothermal flow (no evaporation) : $K \to \infty$, $Q = S = 1$. Shown for three different times, $t = 1$ (——), $t = 10$ (- - - -) and $t = 100$ (– · –).

Figure 6 shows instantaneous interface configurations in the absence of evaporation (isothermal flow). The flow is induced purely by the liquid feeding from above, without any mass loss through the interface. The contact line thus advances monotonically. Figure 7, where the contact-line locations are plotted against time for three different values for the liquid feeding rate Q, seems to indicate that the speed of the advancing contact line reaches an equilibrium value in time. As in the purely evaporative cases, a capillary wave is generated near the bottom, and travels upwards. It is interesting to note that the identical capillarity effect makes the interface configurations for the purely evaporating and the isothermal flows almost mirror images (with respect to the x-axis) of each other. One might expect then that a proper superposition of these two cases would annihilate the capillary wave.

Consider now cases where both the evaporation and the feeding from above are present. It is obvious that if either of these effects is dominant, the interface

https://doi.org/10.1017/S0022112099006758 Published online by Cambridge University Press

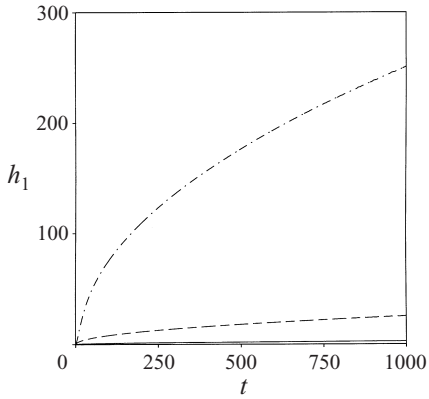


FIGURE 7. Contact-line motion for isothermal flow: $K \to \infty$, $S = G = 1$, and $Q = 0.1$ (——), $Q = 1$ (- - - -) and $Q = 10$ (– · –).

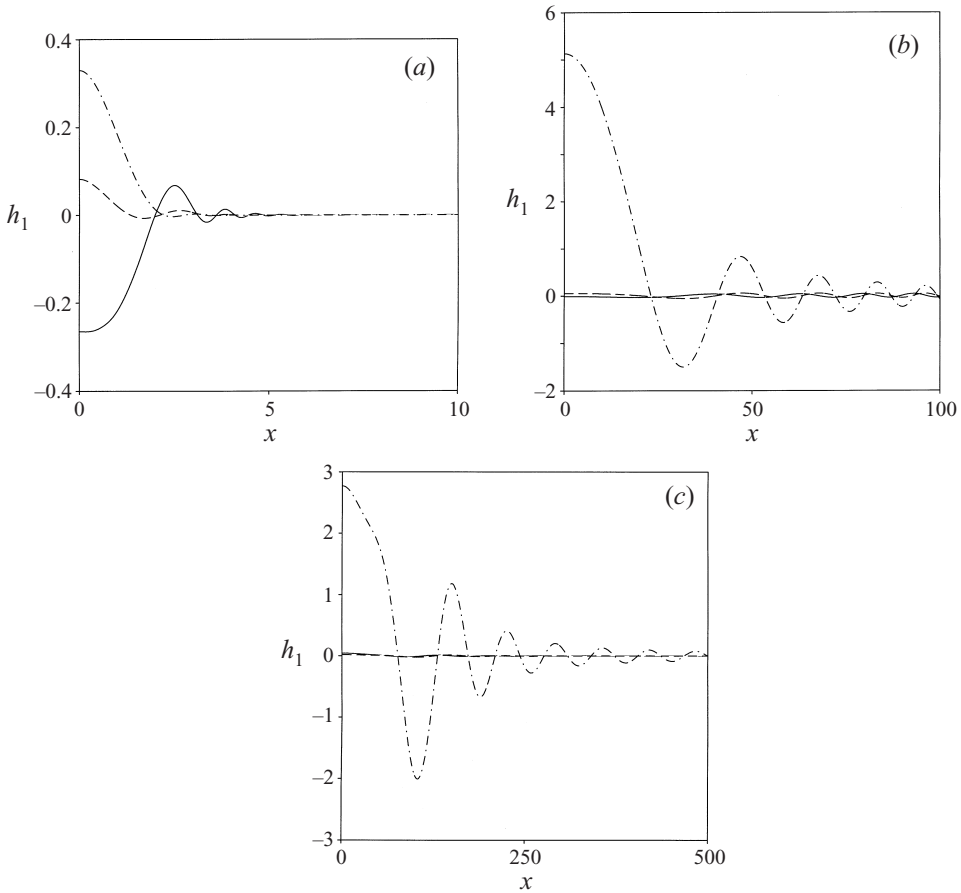


FIGURE 8. Interface configurations when $Q = 1$. $S = G = 1$, and $K = 0$ (——), $K = 1$ (- - - -) and $K = 100$ (– · –). (*a*) $t = 1$; (*b*) $t = 100$; (*c*) $t = 1000$.

configurations and the contact-line dynamics would be similar to the cases already discussed above. Thus consider cases where the two effects compete.

Interface configurations at three different times are shown in figure 8 for three different values of the evaporation rate while the liquid feeding rate is fixed at

https://doi.org/10.1017/S0022112099006758 Published online by Cambridge University Press

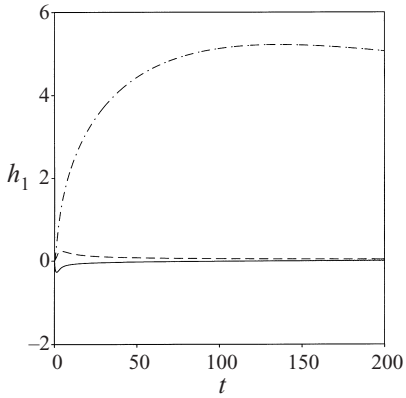


FIGURE 9. Contact-line location against time when $Q = 1$. $S = G = 1$, and $K = 0$ (——), $K = 1$ (- - - -) and $K = 100$ (– · –).

$Q = 1$. In all cases the characteristic capillary wave is generated near the bottom and travels upward, as time progresses. The amplitudes of this wave (height of the humps), however, do not increase monotonically as in the previous cases. For all cases shown, they instead seem to reach maximum values and then become less and less pronounced with time. This transient behaviour also depends on G, the width of the liquid column. When the evaporation is strong ($K = 0$) in comparison with the liquid flow downward accelerating due to gravity, the interface near the contact line recedes initially. The contact line recedes. As the downward liquid flow increases, the rate of net mass loss from the liquid decreases; the liquid feeding from above weakens the interface deflection and forces the contact line to advance. For still larger times, the interface corrugations become less and less conspicuous. When the evaporation is weak ($K = 100$), the effect of liquid feeding is dominant. The liquid tends to wet the bottom gradually until the evaporative effect eventually dominates the wetting process at a large time. The liquid then dewets the bottom gradually. The locations of the contact line for these cases are plotted against time in figure 9. After the contact line reaches a maximum wetting (dewetting) position, it slowly recedes (advances), as discussed above. Integrations for longer times indicate that the decaying behaviour is monotonic for all cases. For the cases shown, the contact line appears to asymptote to an equilibrium value.

A global balance between the mass flux from infinity and that due to evaporation gives a curve separating regions of wetting and dewetting, as shown in figure 10. The total evaporative mass flux at $t = \infty$ can be evaluated as judged by bulk averages

$$I(K) = \int_0^\infty J_1(x, \infty)\mathrm{d}x. \tag{4.1}$$

The net mass balance then gives

$$Q = I(K) \tag{4.2}$$

as the boundary between global mass loss and gain. Along this boundary, liquid fed from above exactly balances the evaporation mass loss, so that the total liquid mass is kept constant. The 'hyperbolic' curve in figure 10 illustrates this boundary for $0 \leqslant K \leqslant 10$. Above this line, the mass flux from infinity exceeds the evaporative mass flux, so that the total mass is constantly increasing. Below the line, the opposite is true. However, since the interface can deform, this global criterion is not predictive

https://doi.org/10.1017/S0022112099006758 Published online by Cambridge University Press

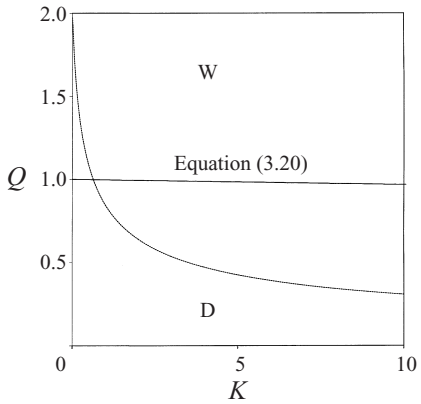


FIGURE 10. Wetting (W) and dewetting (D) regions when $S = 1$.

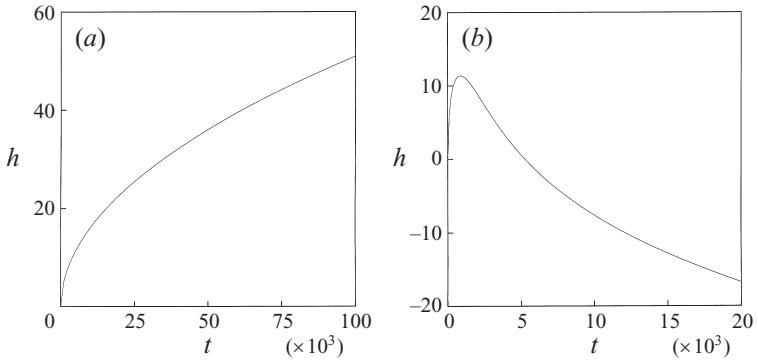


FIGURE 11. Evolution of the contact line when $S = 1$ with (*a*) $K = 0$ and $Q = 1.2$, (*b*) $K = 1000$ and $Q = 0.8$.

of the contact-line motion, which determines the local wetting/dewetting. The correct boundary between wetting (W) and dewetting (D), obtained via integration of the solution (3.20), is shown in figure 10. This line starts at approximately $(0, 1)$ in the (K, Q)-plane, and slopes downward very slowly with the increase of K. The decay of the boundary with the decrease of the evaporative mass flux is much less pronounced than in the global balance. With the increase (decrease) in K, the net evaporative mass loss would decrease (increase), but the evaporative mass flux tends to more (less) localized near the contact line, resulting in contact line motions that are almost insensitive to K.

In figure 11 two cases that show the discrepancy between the global criterion and the local prediction are shown. Case (*a*) is for $(0, 1.2)$ in the (K, Q)-plane. The global criterion predicts a mass loss, and thus dewetting, but the local behaviour shows a monotonic increase of contact line location, and thus wetting. As seen in figure 6, the free-surface elevation due to the mass flux from infinity is most pronounced near the contact line. Although the global evaporative mass flux exceeds the mass flux from infinity, the local evaporative mass loss near the contact line is not sufficient to suppress this pronounced elevation. Wetting results despite gradual net mass loss. Figures 5 and 7 reveal that the sensitivity of contact-line motion to Q is much higher than to K. A small decrease in Q gives a conspicuous decrease in the contact-line

https://doi.org/10.1017/S0022112099006758 Published online by Cambridge University Press

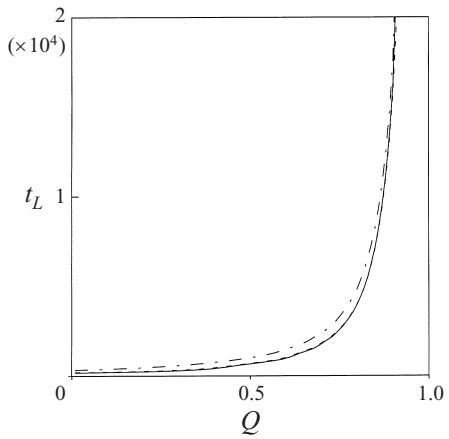


FIGURE 12. The detachment time t_L, in thermal-diffusion scale, when $\epsilon = 0.1$ for $K = 0$ (——), $K = 10$ (- - - -) and $K = 100$ (– · –).

advance, whereas the increase in K does not provide an equally strong decrease in the contact-line recession. As K increases, the surface non-uniformity increases, and the evaporative mass flux is more and more localized near the contact line. Shown in figure 11(b) is a case for $(K, Q) = (1000, 0.8)$, which is far off the range of figure 10, but well within a region of global mass gain but local dewetting. The contact line advances for a while, reaches a maximum, and then recedes monotonically. Dewetting occurs despite gradual net mass gain. Although the global evaporative mass loss is exceeded by the mass influx from infinity, the localized evaporative flux near the contact line is sufficient to overcome the substantially decreased contact-line elevation for the chosen Q.

If the contact line recedes continuously, it can touch the lateral insulating boundary located at $y = -1$. Two contact lines of the liquid finger in figure 1 will merge, and the finger tip would then detach itself from the heated bottom, resulting in a film-boiling state. An extrapolation of the present linear theory can be used to roughly estimate t_L, the detachment time. The time t_L is plotted in figure 12, where the small parameter ϵ is set to 0.1. The range of Q plotted is consistent with the dewetting range shown in figure 10, and varies only slightly with the three values of K chosen. As Q is increased from zero, the mass flux from above increases, and so does t_L. Near $Q = 1$ the boundary between wetting and dewetting exists, where t_L approaches infinity. Increase in K retards the evolution toward film boiling, as expected, but not as efficiently as the increase in Q, for reasons explained above.

5. Concluding remarks

A vertical finger of inviscid liquid heated from a horizontal bottom is studied with a focus on the dynamics of its interface with the vapour phase. The flow is mainly induced by the liquid feeding from above and the evaporation mass flux through the interface.

A uniformly valid solution of a linear problem that accurately describes the evolution of the interface with the moving contact line is obtained in terms of Fourier cosine integrals, which is then evaluated numerically to examine the configurations of the interface under various conditions.

https://doi.org/10.1017/S0022112099006758 Published online by Cambridge University Press

When the liquid feeding from above is dominant, the liquid wets the surface. When the evaporative mass flux is dominant, dewetting occurs. In both situations, capillary waves are generated near the contact line, and propagate away from it. The interface corrugations, or the amplitudes of the capillary wave, do not grow monotonically when the liquid feeding and the evaporation mass flux are comparable. They reach maxima, and then decay.

The parametric regions for wetting and dewetting are identified. It is shown that these regions cannot be identified by a simple global mass balance. Local dynamics dictates the contact-line motion and thus the wetting/dewetting behaviour. The global mass balance provides conditions of the mass influx from above sufficient for wetting when the evaporative mass flux is strong (small K), whereas it provides only necessary conditions for wetting otherwise.

The present study is prompted by the necessity of a more rigorous analysis for the dynamic behaviour of the vapour/liquid interface in transition and film boiling processes. The one-sided inviscid model described here must be generalized further to yield more precise results. In a more realistic model, the mass influx from above, described by the parameter Q here, must be coupled with the flow dynamics near the contact line.

This study is supported by the Engineering Research Program of the Office of Basic Energy Sciences, US Department of Energy. The authors gratefully acknowledge Mr Chang H. Park of Yeungnam University for his help with the figure preparation.

REFERENCES

Anderson, D. M. & Davis, S. H. 1995 The spreading of volatile liquid droplets on heated surfaces. *Phys. Fluids* **7**, 248–265.

Burelbach, J. P., Bankoff, S. G. & Davis, S. H. 1988 Nonlinear stability of evaporating/condensing liquid films. *J. Fluid Mech.* **195**, 463–494.

Carey, P. van 1992 *Liquid-Vapour Phase Change Phenomena.* Hemisphere.

Cooper, M. G & Lloyd, A. J. P. 1969 The microlayer in nucleate pool boiling. *Intl J. Heat Mass Transfer* **12**, 895–913.

Dhir, V. K. 1998 Boiling heat transfer. *Ann. Rev. Fluid Mech.* **30**, 365–401.

Joo, S. W., Messiter, A. F. & Schultz, W. W. 1990 An analysis of the initial-value wavemaker problem. *J. Fluid Mech.* **214**, 161–183.

Miles, J. W. 1991 On the initial-value problem for a wavemaker. *J. Fluid Mech.* **229**, 589–601.

Moore, F. D. & Mesler, R. B. 1961 The measurement of rapid surface temperature fluctuations during nucleate boiling of water. *AIChE J.* **7**, 620–624.

Panzarella, C. H. 1998 Nonlinear dynamics in horizontal film boiling. PhD thesis, Northwestern University, Evanston.

Peregrine, D. H. 1972 Flow due to a vertical plate moving in a channel. Unpublished note.

Prosperetti, A. & Plesset, M. S. 1984 The stability of an evaporating liquid surface. *Phys. Fluids* **27**, 1590–1602.

Roberts, A. J. 1987 Transient free-surface flows generated by a moving vertical plate. *Q. J. Mech. Appl. Maths* **40**, 129–158.

Rohsenow, W. M. 1971 Boiling. *Ann. Rev. Fluid Mech.* **3**, 211–236.

Snyder, N. R. & Edwards, D. K. 1956 Summary of conference on bubble dynamics and boiling heat transfer. *Memo* 20-137, pp. 14–15. Jet Propulsion Lab., Pasadena, CA.

https://doi.org/10.1017/S0022112099006758 Published online by Cambridge University Press

Wilson, S. K., Davis, S. H. & Bankoff, S. G 1999 The unsteady expansion and contraction of a long two-dimensional vapour bubble between superheated or subcooled parallel plates. *J. Fluid Mech.* **391**, 1–27.

Witte, L. C. & Lienhard, J. H. 1982 On the existence of two 'transition' boiling curves. *Intl J. Heat Mass Transfer* **25**, 771–779.

https://doi.org/10.1017/S0022112099006758 Published online by Cambridge University Press